The *Brucella* effector BspL targets the ER-associated degradation (ERAD) pathway and delays bacterial egress from infected cells

Jean-Baptiste Luizet[a], Julie Raymond[a], Thais Lourdes Santos Lacerda[a], Emeline Barbieux[b,c], Stanimir Kambarev[d], Magali Bonici[a], Frédérique Lembo[e], Kévin Willemart[b], Jean-Paul Borg[e,f], Jean Celli[d], Francine C. A. Gérard[a], Eric Muraille[b,c], Jean-Pierre Gorvel[g], and Suzana P. Salcedo[a,1]

[a]Laboratory of Molecular Microbiology and Structural Biochemistry, CNRS UMR5086, Université de Lyon, 69367 Lyon, France; [b]Department of Biology, Research Unit in Microorganisms Biology, Namur Research Institute for Life Sciences, 5000 Namur, Belgium; [c]Laboratory of Parasitology, Université Libre de Bruxelles Centre for Research in Immunology (UCRI), Université Libre de Bruxelles, 6041 Gosselies, Belgium; [d]Paul G. Allen School for Global Animal Health, Washington State University, Pullman, WA 99164; [e]Equipe labellisée Ligue 'Cell Polarity, Cell Signaling and Cancer', Centre de Recherche en Cancérologie de Marseille, Institut Paoli-Calmettes, Aix-Marseille Université, CNRS, INSERM, 13009 Marseille, France; [f]Institut Universitaire de France, 75231 Paris, France; and [g]Centre d'Immunologie de Marseille-Luminy, CNRS, INSERM, Aix-Marseille Université, 13009 Marseille, France

Edited by Ralph R. Isberg, Tufts University School of Medicine, Boston, MA, and approved June 21, 2021 (received for review March 18, 2021)

Perturbation of the endoplasmic reticulum (ER), a central organelle of the cell, can have critical consequences for cellular homeostasis. An elaborate surveillance system known as ER quality control ensures that cells can respond and adapt to stress via the unfolded protein response (UPR) and that only correctly assembled proteins reach their destination. Interestingly, several bacterial pathogens hijack the ER to establish an infection. However, it remains poorly understood how bacterial pathogens exploit ER quality-control functions to complete their intracellular cycle. *Brucella* spp. replicate extensively within an ER-derived niche, which evolves into specialized vacuoles suited for exit from infected cells. Here we present *Brucella*-secreted protein L (BspL), a *Brucella abortus* effector that interacts with Herp, a central component of the ER-associated degradation (ERAD) machinery. We found that BspL enhances ERAD at the late stages of the infection. BspL targeting of Herp and ERAD allows tight control of the kinetics of autophagic *Brucella*-containing vacuole formation, delaying the last step of its intracellular cycle and cell-to-cell spread. This study highlights a mechanism by which a bacterial pathogen hijacks ERAD components for fine regulation of its intracellular trafficking.

Brucella | ERAD | Herp | trafficking

The endoplasmic reticulum (ER) is the largest organelle in the cell and plays numerous functions vital for maintaining cellular homeostasis. It is the primary site for protein synthesis of both secreted and integral membrane proteins and the export of newly synthesized proteins to other cellular organelles. Disturbance or saturation of the ER's folding-capacity leads to a complex stress response that helps cells recover homeostasis or, if necessary, commit them to death. The ER relies on a surveillance system known as ER quality control (ERQC) that ensures the processing of misfolded, misassembled, or metabolically regulated proteins (1). Once retained in the ER, most of these proteins are retrotranslocated into the cytosol to be ubiquitinated and degraded by the proteasome, a process known as ER-associated degradation (ERAD) (2). In response to ERQC perturbations, ER stress ensues, and cells activate a set of interconnected pathways that are collectively referred to as the unfolded protein response (UPR) (3).

The homocysteine-inducible ER stress protein (Herp) is an ER membrane protein that is highly up-regulated during ER stress by all UPR branches (4, 5). Herp is a critical component of ERQC that plays a protective role in ER stress conditions (6, 7). It is an integral part of the ERAD pathway, enhancing the ER's protein loading and folding capacities. In addition, it acts as a hub for membrane association of ERAD machinery components, stabilizing their interactions with substrates at ERQC sites (8) and facilitating their retrotranslocation (9). Furthermore, as Herp is also associated with the proteasome, it may help deliver specific retrotranslocated substrates to the proteasome for degradation (10, 11).

Given its importance for cellular homeostasis, ERQC represents a prime target for microbial pathogens. Indeed, a growing number of bacterial pathogens have been shown to modulate UPR (12). This is the case of *Brucella* spp., a facultative intracellular pathogen that causes a major zoonosis prevalent worldwide. *Brucella abortus* has been shown to induce UPR (13, 14), and more specifically, the IRE1 pathway, contributing to enhanced inflammation, a process particularly relevant in the context of colonization of the placenta and abortion (15). However, activation of IRE1 also impacts *Brucella* trafficking and subsequent *Brucella* multiplication (14, 16). After cellular uptake, *Brucella* resides in a membrane-bound compartment designated the endosomal *Brucella*-containing vacuole (eBCV), which transiently interacts with the endocytic pathway (17). Bacteria can then establish an ER-derived compartment suited for multiplication (replicative, or rBCV) (18). UPR induction by *Brucella* is necessary for this trafficking step, as the formation of rBCVs is dependent on

Significance

Intracellular bacterial pathogens rely on dedicated systems to inject effector proteins into host cells and cause disease. This is the case for *Brucella abortus*, which causes brucellosis, one of the world's most prevalent zoonotic diseases. We have found one such effector that can control the intracellular fate of *Brucella* by hijacking the machinery of the endoplasmic reticulum generally used by our cells to degrade misfolded or unwanted proteins. This bacterial effector works to slow down the formation of a specialized vacuole that enables *Brucella* to exit from the cell and infect neighboring cells. This delay ultimately allows the bacteria extra time for extensive intracellular multiplication, an essential feature of its virulence.

Author contributions: J.-B.L., J.R., T.L.S.L., S.K., J.-P.B., J.C., F.C.A.G., E.M., J.-P.G., and S.P.S. designed research; J.-B.L., J.R., T.L.S.L., E.B., S.K., M.B., F.L., K.W., J.C., F.C.A.G., and S.P.S. performed research; J.-B.L., J.R., T.L.S.L., E.B., S.K., F.L., J.-P.B., J.C., F.C.A.G., E.M., J.-P.G., and S.P.S. analyzed data; and J.-B.L., J.C., E.M., J.-P.G., and S.P.S. wrote the paper.

The authors declare no competing interest.

This article is a PNAS Direct Submission.

[1]To whom correspondence may be addressed. Email: suzana.salcedo@ibcp.fr.

This article contains supporting information online at https://www.pnas.org/lookup/suppl/doi:10.1073/pnas.2105324118/-/DCSupplemental.

Published August 5, 2021.

IRE1 activation via the ERES-localized protein Yip1A (19). Once rBCVs are established, *Brucella* is capable of extensive intracellular replication without induction of cell death. Instead, at the late stages of the intracellular cycle, rBCVs reorganize to form large autophagic vacuoles (aBCVs) that will mediate bacterial exit from infected cells (20). The bacterial factors behind the switch between rBCVs and aBCVs remain uncharacterized.

Brucella relies on a type 4 secretion system (T4SS), encoded by the *virB* operon to translocate bacterial effectors into host cells and directly modulate cellular functions, including the biogenesis of rBCVs (21–23) and formation of aBCVs (24). However, only a few effectors have been characterized to date. The T4SS is also implicated in UPR induction during infection, and a subset of these effectors modulate ER-associated functions. VceC interacts with the ER chaperone BiP to activate the IRE1 pathway, which results in NOD1/NOD2 activation and up-regulation of inflammatory responses (13, 15). *Brucella*-secreted protein (Bsp) A, BspB, and BspF have all been implicated in blocking ER secretion (25). In particular, BspB interacts with the conserved oligomeric Golgi (COG) complex to redirect vesicular trafficking toward the rBCVs (26).

In this study, we identify a T4SS effector of *B. abortus* that we designate as *Brucella*-secreted protein L (BspL) that targets Herp, a component of the ERAD machinery. BspL enhances ERAD and delays the formation of aBCVs, preventing early bacterial release from infected cells to potentially ensure optimal intracellular proliferation prior to aBCV formation and help to maintain cell-to-cell spread efficiency.

Results

BspL Is a *Brucella* T4SS Effector Protein. Bacterial effectors often contain domains and motifs that are characteristic of eukaryotic proteins. For example, some contain a carboxyl-terminal CAAX tetrapeptide motif (C corresponds to cysteine, A to aliphatic amino acids, and X to any amino acid) that serves as a lipidation site to facilitate membrane attachment (27, 28). Previous work highlighted several *Brucella*-encoded proteins with putative CAAX motifs (29), which could be translocated effectors. In this study, we focused on one of these proteins encoded by the gene BAB1_1533 (YP_414899.1), which we have designated BspL (*SI Appendix*, Fig. S1*A*).

We first determined if BspL was translocated into host cells during infection. We constructed a strain expressing BspL fused to the C terminus of the TEM1 β-lactamase and infected RAW macrophage-like cells for different time-points. We included the T4SS effector VceC as a positive control (30), which showed the highest secretion level at 24 h postinfection (Fig. 1*A*). We found that TEM1-BspL was secreted into host cells as early as 4 h postinfection, increasing at 12 and 24 h postinfection (Fig. 1*A*). This phenotype was dependent on the T4SS since a Δ*virB9* mutant strain did not show any coumarin fluorescence (Fig. 1 *A* and *B*), despite expressing equivalent levels of TEM1-BspL to the wild-type strain, as measured by Western blot in the inocula (Fig. 1*C*). Together, these results show BspL is a T4SS effector.

BspL Is Not Involved in the Establishment of an ER-Derived Replication Niche but Is Implicated in the Induction of ER Stress During Infection. BspL is well conserved in the *Brucella* genus. It is 170-amino acids long (*SI Appendix*, Fig. S1*A*), ~19 kDa, and does not share homology to eukaryotic nor other bacterial proteins. Its nucleotide sequence encodes for a predicted Sec-dependent secretion signal, a feature found in other *Brucella* effectors (31). To gain insight into the function of BspL, we ectopically expressed HA-, myc-, or GFP-tagged BspL in HeLa cells. We found BspL accumulated in the ER, as seen by the colocalization with calnexin (Fig. 1*D* and *SI Appendix*, Fig. S1 *B* and *C*), an ER chaperone. Deletion of the C-terminal tetrapeptide sequence did not affect the ER localization of BspL in transfection (*SI Appendix*, Fig. S1*B*, *Lower*), as

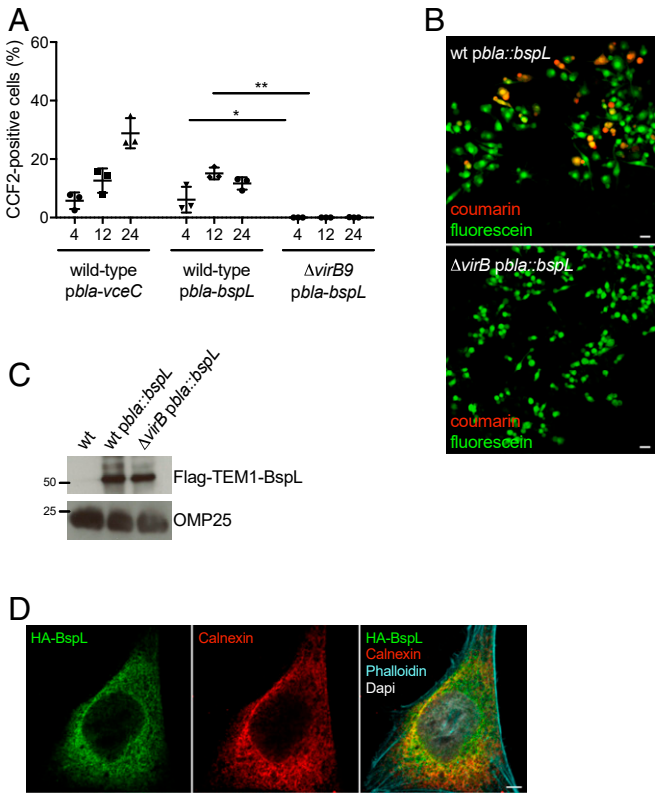

Fig. 1. BspL is a T4SS effector translocated into host cells during *B. abortus* infection. (*A*) Macrophage-like RAW cell line was infected with *B. abortus* carrying a plasmid encoding for *bla* fused with *bspL* (p*bla-bspL*) to enable expression of TEM-BspL. Cells were infected with either wild-type *B. abortus* or Δ*virB9* carrying this plasmid. A positive control of wild-type expressing *bla-vceC* was included. At 4, 12, or 24 h postinfection, cells were incubated with fluorescent substrate CCF2-AM, fixed and the percentage of cells with coumarin emission quantified. More than 1,000 cells were quantified for each condition from three independent experiments, and data represent means ± SD, $n = 3$. Kruskal–Wallis with Dunn's multiple comparisons test was used and $P = 0.0375$ between wild-type p*bla-bspL* and Δ*virB9* p*bla-bspL* at 4 h (*) and 0.0046 at 12 h (**). Not all statistical comparisons are shown. (*B*) Representative images of cells infected for 24 h with *B. abortus* wild-type or Δ*virB9* carrying p*bla-bspL*. Cells were incubated with CCF2, and the presence of translocated TEM1-BspL was detected by fluorescence emission of coumarin (red). (*C*) The expression of TEM1-BspL in the inocula of wild-type and Δ*virB9* strains was controlled by Western blotting. The membrane was probed with an anti-Flag antibody (*Upper*) or anti-Omp25 (*Lower*) as a loading control. A sample from wild-type without the plasmid was included as a negative control. Molecular mass is indicated (kDa). (*D*) Confocal microscopy image showing the intracellular localization of HA-BspL expressed in HeLa cells labeled with an anti-HA antibody (green) and ER marker calnexin (red). Phalloidin (cyan) was used to label the actin cytoskeleton and Dapi (white) for the nucleus. (Scale bars, 5 μm.)

it significantly overlapped with the full-length protein when coexpressed in the same cell (*SI Appendix*, Fig. S1*C*).

Our observations suggest BspL is part of a growing number of ER-associated *Brucella* effectors (13, 25). We, therefore, investigated if BspL shared any of the ER modulatory functions described for other effectors, notably interference with ER secretion as BspB (25, 26) or induction of ER stress as VceC (13, 15).

To determine the impact of BspL on host protein secretion, we used the secreted embryonic alkaline phosphatase (SEAP) as a reporter system. We chose to work with HA-BspL to directly compare with previously published HA-BspB that blocks ER secretion and HA-BspD as a negative control (25). Expression of the GDP-locked allele of the small GTPase Arf1[T31N], known to block the early secretory pathway, was used as a control for

efficient inhibition of secretion (*SI Appendix*, Fig. S1*D*). As previously reported, we found that the expression of HA-BspB drastically reduced SEAP secretion (*SI Appendix*, Fig. S1*D*). In contrast, the effect of HA-BspL effect was equivalent to HA-BspD, previously reported not to affect host protein secretion (25).

We next investigated whether ER targeting of BspL was accompanied by an activation of the UPR, an important feature of *Brucella* pathogenesis (15, 16, 19). IRE1 is the main pathway activated (13), leading to splicing of the mRNA encoding the transcription factor X-box-binding protein 1 (XBP1). The other branch of the UPR that may also be of relevance in *Brucella* infection (14) is dependent on PERK and leads to the up-regulation of the transcription factor C/EBP-homologous protein (CHOP). We therefore monitored *XBP1s* and *CHOP* transcript levels following ectopic expression of HA-BspL, in comparison to HA-VceC, an established ER stress inducer (13), and HA-BspB, known not to induce ER stress (25). Treatment with tunicamycin, a chemical ER stress inducer, was also included. We found that overexpression of HA-BspL in HeLa cells induced an increase of both *XBP1s* and *CHOP* transcription (*SI Appendix*, Fig. S2 *A* and *B*).

We next monitored the levels of *XBP1s* and *CHOP* transcripts during infection. Since the rate of infected cells is too low to detect ER stress in HeLa cells, these experiments were performed with an immortalized cell line of bone marrow-derived macrophages (iBMDM). Macrophages infected with a Δ*bspL* mutant for 48 h showed decreased *XBP1s* transcript levels compared to the wild-type (*SI Appendix*, Fig. S2*C*). Furthermore, the wild-type phenotype was fully restored by expressing a chromosomal copy of *bspL* in the Δ*bspL* strain (*SI Appendix*, Fig. S2*C*), confirming that BspL contributes toward the induction of the IRE1 branch of the UPR. We did not observe an increase in *CHOP* transcript levels in iBMDM infected with the wild-type or *bspL* strains compared to the mock-infected cells (*SI Appendix*, Fig. S2*D*), suggesting that *B. abortus* does not significantly induce the PERK-dependent branch of the UPR at this stage of the infection.

As UPR has been implicated in establishing rBCVs (19) and intracellular replication of *Brucella* (14, 16, 19), we investigated the intracellular fate of a *B. abortus* 2308 strain deleted for *bspL* in comparison with the wild-type. We found that the Δ*bspL* strain replicated as efficiently as the wild-type in both iBMDM (*SI Appendix*, Fig. S3*A*) and HeLa cells (*SI Appendix*, Fig. S3*B*). No apparent differences in intracellular trafficking were observed at 24 and 48 h postinfection, with Δ*bspL* BCVs positive for calnexin in both cell types (*SI Appendix*, Fig. S3 *D* and *F*). As iBMDM have not previously been used to study *Brucella* infections we quantified the percentage of BCVs positive for calnexin and the lysosomal-associated membrane protein 1 (LAMP1) in comparison with the wild-type at 24 and 48 h postinfection (*SI Appendix*, Fig. S3 *G* and *H*, respectively). The wild-type strain in this cellular model behaved as expected.

BspL Interacts with Herp, a Key Component of ERQC. To gain insight into the function of BspL, we set out to identify its interacting partners. A yeast two-hybrid screen identified seven candidates: the eukaryotic translation initiation factor 4A2 (EIF4A2), the pyruvate dehydrogenase-β (PDHB), the MTR 5-methyltetrahydrofolate-homocysteine methyltransferase, the Bcl2-associated athanogene 6 (BAG6), the ARMCX3 armadillo repeat-containing protein (Alex3), the homocysteine-inducible ER protein with ubiquitin-like domain (Herpud1 or Herp), and the Ubiquilin2 (Ubqln2).

Given our previous results for BspL showing ER localization and induction of UPR, we focused on Alex3, Herp, and Ubiquilin2, which are rarely present or even absent in the database of false positives for this type of screen (https://reprint-apms.org/). Alex3 is a mitochondrial outermembrane protein implicated in the regulation of mitochondrial trafficking (32). As ER and mitochondria extensively interact, Alex3 could constitute an interesting target. Herp is an ER membrane protein playing a role in both the UPR and the ERAD system, whereas Ubiquilin2 is implicated in both the proteasome and ERAD and, interestingly, shown to interact with Herp (33). To test the specificity of these targets, we carried out an endogenous coimmunoprecipitation (co-IP) in cells expressing HA-BspL. As controls for detecting nonspecific binding, we also performed co-IP experiments from cells expressing two other ER-targeting effectors, HA-BspB and HA-VceC. Eluted samples were probed with antibodies against Alex3, Ubiquilin2, or Herp to detect the interactions. We found that Alex3 was coeluted with all three effectors, suggesting a potentially nonspecific interaction with the effectors or the resin itself (Fig. 2*A*). In contrast, no interactions were observed with Ubiquilin2, which was detected only in the flow-through fractions. However, we found that endogenous Herp specifically coeluted with HA-BspL and not the other effectors (Fig. 2*A*), suggesting Herp and BspL form a complex within host cells. To confirm these results, we coexpressed GFP-BspL with Flag-Herp in HeLa cells and carried out a co-IP. Despite much higher GFP expression levels, only GFP-BspL could co-IP Flag-Herp (Fig. 2*B*), confirming they are part of the same complex. Taken together with the yeast two-hybrid data, we can conclude that BspL directly interacts with Herp. Consistently, overexpressed BspL colocalized with Herp by microscopy (Fig. 2*C*).

BspL Facilitates Degradation of T Cell Receptor-α via ERAD, Independently of ER Stress. Herp is a critical component of ERAD, strongly up-regulated upon ER stress (5). During *Brucella* infection, and despite the induction of UPR, we observed only a slight

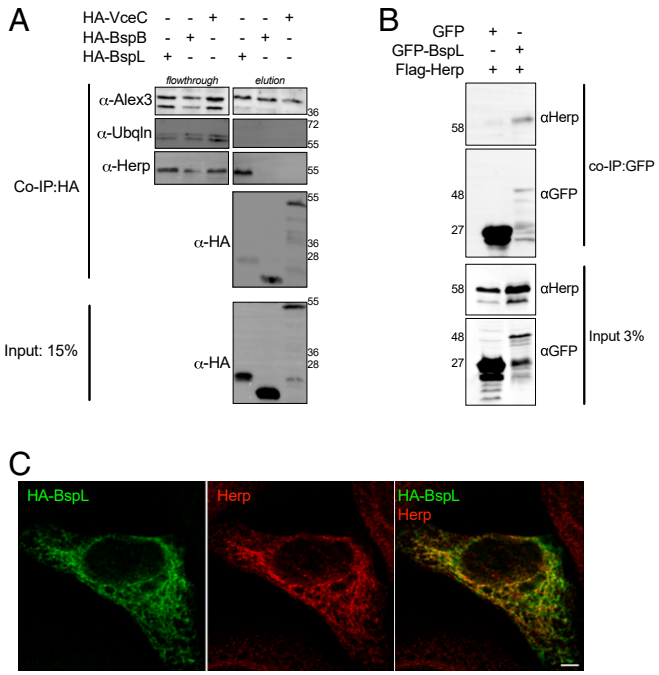

Fig. 2. BspL specifically interacts with the ERAD component Herp. (*A*) co-IP from cell extracts expressing either HA-BspL, HA-BspB, and HA-VceC using HA-trapping beads. Flow-through and elutions were probed with antibodies against Alex3, Ubiquilin (Ubqln), and Herp in succession. The level of each effector bound to the beads was revealed with an anti-HA antibody and 15% of the input used for the co-IP shown (at the bottom). Molecular mass is indicated (kDa). (*B*) Co-IP assay from cells expressing GFP-BspL and Flag-Herp. GFP was used as a control for nonspecific binding. The co-IP was revealed using an anti-Herp antibody, the fraction bound to GFP-trapping beads with an anti-GFP antibody, and the inputs (shown on the *Lower* two images) with anti-Herp and anti-GFP antibodies. Molecular mass is indicated (kDa). (*C*) Representative confocal micrograph of HeLa cells expressing HA-BspL (green) and labeled for Herp (red). (Scale bar, 5 μm.)

MICROBIOLOGY

up-regulation of *HERP* transcripts that was not statistically significant (*SI Appendix*, Fig. S4*B*). Although we could not detect Herp in macrophages with the antibodies tested, we did not observe any increase in Herp protein levels in infected HeLa cells. Indeed, inhibition of Herp using small-interfering RNA (siRNA) (*SI Appendix*, Fig. S4*C*) showed that ER stress induced following ectopic expression of BspL was not dependent on Herp (*SI Appendix*, Fig. S4 *D* and *E*), suggesting BspL interaction with Herp is mediating other functions in the cell.

Therefore, we next investigated if BspL could directly impact ERAD. We used expression of T cell receptor-α (TCRα) as reporter system, as this type I transmembrane glycoprotein is a canonical, quickly degraded ERAD substrate (34, 35). Cycloheximide treatment for 4 h was used to block protein synthesis, preventing the replenishment of TCR pools and allowing visualization of ERAD-mediated degradation of TCRα. When HEK-293T cells, which do not naturally express TCR, were transfected with HA-TCRα and treated with cycloheximide, a decrease in HA-TCRα was observed, indicative of degradation (Fig. 3*A*, red arrow). Strikingly, expression of BspL induced substantial degradation of TCRα (Fig. 3*A*). This was accompanied by the appearance of a faster migrating band at around 25 kDa (Fig. 3*A*, blue arrow) that nearly disappears upon cycloheximide treatment, suggesting the proteasome efficiently degrades this TCRα peptide. It is important to note that the 25-kDa band is also present when HA-TCRα is expressed alone (lane 2 of Fig. 3*A*, blue arrow), suggesting it is a natural intermediate of HA-TCRα degradation.

As the TCRα subunit undergoes *N*-glycosylation in the ER, we wondered if the faster-migrating band of TCRα induced by BspL corresponded to a nonglycosylated form of TCRα. We, therefore, treated samples with EndoH, which deglycosylates peptides. Upon EndoH treatment, we observed deglycosylated HA-TCRα, also visible when BspL is expressed (*SI Appendix*, Fig. S5*A*, black arrow). The dominant TCRα band induced upon BspL expression (around 25 KDa) (*SI Appendix*, Fig. S5*A*, blue arrow) is not sensitive to EndoH. This may therefore correspond to a natural truncated nonglycosylated form of HA-TCRα. Consistently, this band is also present in the absence of BspL (lane 1, Fig. 3*B*, blue arrow). These results suggest that all visible TCRα bands in the presence of BspL are EndoH-resistant and therefore correspond to deglycosylated TCRα.

To control if the effect of BspL on enhanced TCRα degradation is a side-effect of ER stress, cells were treated with tauroursodeoxycholic acid (TUDCA), which strongly inhibited both *XBP1s* and *CHOP* transcript levels induced by either tunicamycin, BspL, or VceC (*SI Appendix*, Fig. S4 *F* and *G*). In the presence of TUDCA, BspL still caused HA-TCRα degradation showing this is occurring in an ER stress-independent manner (Fig. 3*B*).

Finally, to ensure the observed BspL effects are not specific to a single ERAD substrate or due to an indirect impact on TCRα trafficking, we tested an additional ERAD reporter. HeLa cells were transfected to produce the soluble ERAD substrate Null Hong Kong (NHK)–α1-antitrypsin with either Myc-BspL or Myc-VceC. In contrast to VceC, BspL induced significant degradation of NHK, confirming its ERAD activator capacity (*SI Appendix*, Fig. S5*B*).

BspL Induces ERAD During the Late Stages of *B. abortus* Infection. To determine if BspL induces ERAD during infection, we took advantage of the 293T.FluERAD cells that express the SS-ddV1Z ERAD substrate. This substrate includes the N-terminus sequence of Venus, which fluoresces only after being translocated in the cytosol thanks to the presence of its complementary cytosolic C-terminal Venus sequence. Importantly, fluorescence is only observed when this reporter properly traffics to the ER, is subsequently glycosylated and retrotranslocated in the cytosol, and finally deglycosylated (36), allowing us to monitor the impact of *Brucella* on ERAD at different stages of the infection.

After 6 h of incubation with the proteasome inhibitor MG132, nuclear fluorescence can be observed in noninfected cells (Fig. 3 *C* and *D*), as previously reported (36). As this process is dependent on deglycosylation, treatment with the PNGase inhibitor (zVAD-fmk) significantly abolishes fluorescence accumulation (36) (Fig. 3*C*). As expected, in the absence of the proteasome inhibitor MG132, no fluorescence was observed in any of the conditions, including cells infected with either wild-type, Δ*bspL*, or the complemented strains (Fig. 3 *C* and *D*). When MG132 was added at 18 h postinfection and SS-ddV1Z fluorescence quantified 6 h later, we did not observe any differences in the levels of ERAD (*SI Appendix*, Fig. S5*C*). However, when the proteasome was blocked at 42 h postinfection and fluorescence monitored 6 h after, we observed that the wild-type–infected cells showed significantly higher levels than those infected with Δ*bspL* (Fig. 3 *C* and *D*). We could fully complement this phenotype, suggesting that BspL contributes to ERAD activation at the late stages of *Brucella* infection (Fig. 3*C*). Treatment with zVAD-fmk strongly reduced SS-ddV1Z fluorescence for all strains, suggesting the observed phenotypes were dependent on deglycosylation. Therefore, traffic, entry, and exit of the substrate in the ER are not affected by BspL. Together, these data indicate that BspL induces ERAD, implicating this process in *Brucella* pathogenesis.

BspL Delays Bacterial Egress from Infected Cells. As we only observed the effect of BspL on ERAD at late stages of the infection, without any impact on the formation of rBCVs, we decided to test whether BspL could be involved in subsequent steps of the intracellular trafficking. The late stage of the intracellular cycle of *Brucella* relies on the induction of specific autophagy proteins to enable the formation of aBCVs characterized as large $LAMP1^+$ vacuoles containing multiple bacteria (20). In this study, aBCVs were defined as $LAMP1^+$ and $calnexin^-$ vacuoles with a minimum of four bacteria to distinguish from potential BCVs that failed to fuse with the ER and establish rBCVs. Consistent with what was previously reported (20), we did not observe the presence of a significant number of wild-type aBCVs at 24 h. In our experimental conditions, aBCVs could be observed in iBMDM infected for 65 h with wild-type *B. abortus* (Fig. 4 *A* and *B*). We, therefore, investigated if BspL was involved in the formation of aBCVs. Strikingly, a few Δ*bspL* aBCVs could be detected as early as 24 h, with nearly 30% of infected cells showing aBCVs at 48 h postinfection compared to less than 10% for wild-type infected cells (Fig. 4 *B* and *C*). Importantly, complementation of the Δ*bspL* strain fully restored the wild-type phenotype. These results show that BspL is involved in delaying the formation of aBCVs during *B. abortus* macrophage infection. As aBCV formation was previously linked to *Brucella* exit from infected cells and spread to neighboring cells (20, 24), we next searched for reinfection events. Wild-type–infected iBMDM at 48 h postinfection showed none or few signs of reinfection, with most cells showing extensive perinuclear ER-like distribution of bacteria (Fig. 4*D*). In contrast, imaging of Δ*bspL*-infected iBMDM at the same time point revealed cells with single bacteria or a single aBCV (Fig. 4*D*), suggestive of reinfection and reminiscent of what was previously described for wild-type *B. abortus* at 72 h postinfection (20).

To confirm these results, we quantified bacterial egress and cell-to-cell spread in infected HeLa cells, as previously described (24). Analysis of colony-forming unit (CFU) counts in supernatants of infected cells (incubated for 24 h without antibiotics) revealed a higher number of Δ*bspL* bacteria at 48 h postinfection in comparison with the wild-type (Fig. 4*E*), suggesting earlier release from *B. abortus*–infected cells in the absence of BspL. We next incubated infected cells with new cells prelabeled with Cell Tracker green for 24 h in the absence of antibiotics. We found higher levels of reinfection for the Δ*bspL* strain in comparison

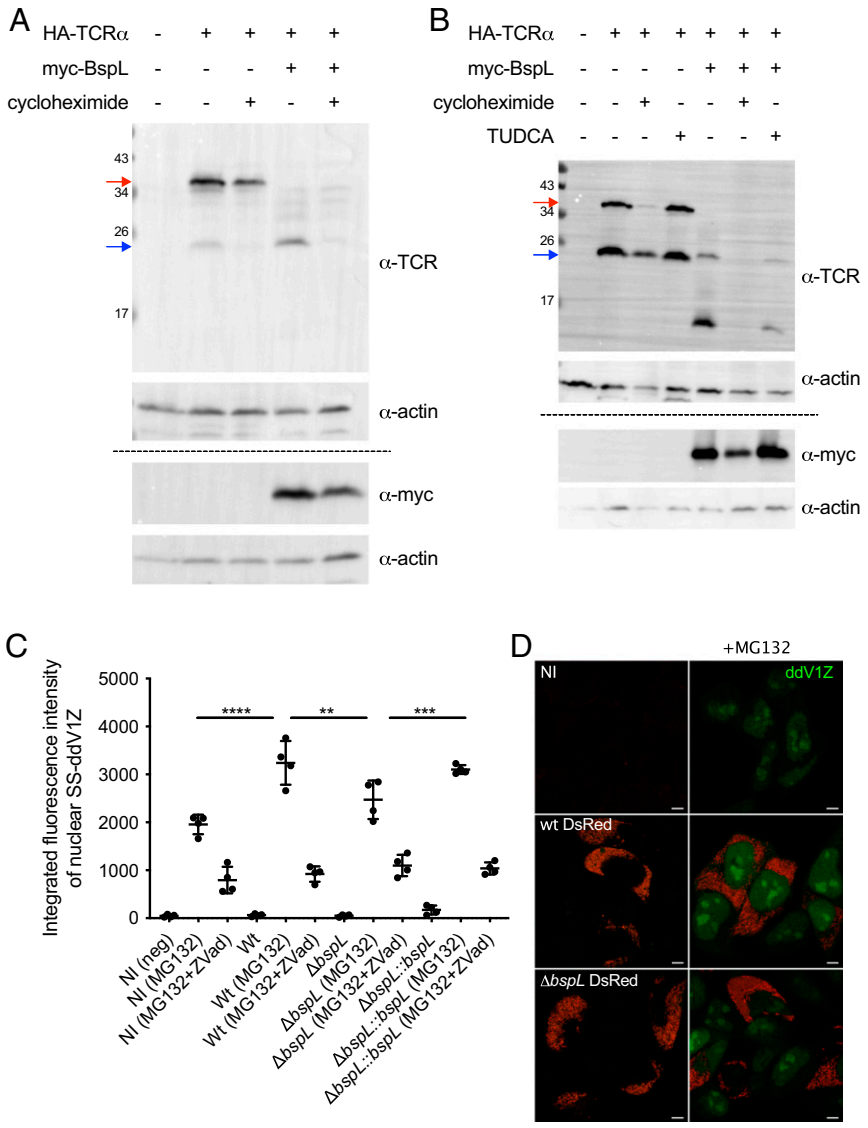

Fig. 3. BspL enhances ERAD degradation of TCRα. (*A*) HEK 293T cells were transfected with HA-TCRα in the absence or presence of myc-BspL for 24 h. Where indicated, cells were treated with 50 μg/mL cycloheximide for the last 4 h. The blot was probed first with an anti-TCR antibody followed by anti-actin. The same samples were loaded onto a separate gel (separated by a dashed line) for probing with an anti-myc and anti-actin to confirm the expression of myc-BspL. Molecular mass is indicated (kDa), and the relevant bands described in the text are highlighted with different colored arrows. (*B*) HEK 293T cells were transfected with HA-TCRα in the absence or presence of myc-BspL for 24 h. Where indicated, cells were treated with 50 μg/mL cycloheximide for the last 6 h or 0.5 nM of TUDCA for 22 h. The blot was probed first with an anti-TCR antibody followed by anti-actin. The same samples were loaded onto a separate (separated by a dashed line) for probing with an anti-myc and anti-actin to confirm the expression of myc-BspL. Molecular mass is indicated (kDa), and the relevant bands described in the text are highlighted with different colored arrows. (*C*) HEK293T.FluERAD cells that express the SS-ddV1Z ERAD substrate were either mock-infected or inoculated with either wild-type, Δ*bspL*, or the complemented Δ*bspL*::*bspL* strains for 42 h and, when indicated, either treated with MG132 or in combination with ZVad for 6 h before fixation. At least 30 cells were analyzed per condition and per experiment to measure the integrated nuclear fluorescence intensity. Data correspond to means ± SD from three independent experiments. Not all comparisons are shown. (*D*) Representative images of HEK293T.FluERAD cells either noninfected (NI) or inoculated with wild-type or Δ*bspL*-expressing DSRed for 48 h. The left column corresponds to untreated cells and the right column following MG132 treatment for 6 h to block the proteasome. The fluorescence of ssV1Z (green) is primarily visible in the nucleus after MG132 treatment. (Scale bars, 5 μm.)

with the wild-type, particularly at 65 h postinfection (Fig. 4*F*). Together, these results suggest that BspL contributes to a delay in forming aBCVs, resulting in deferred bacterial egress and cell-to-cell spread. To determine if early egress impacts host colonization, we carried out in vivo experiments using a *Brucella* pulmonary infection model in mice. No significant differences were observed between the wild-type and Δ*bspL* bacterial counts in the lung at 2 or 5 d postinoculation (*SI Appendix*, Fig. S6).

In view of our results and the fact that BspL interacts with Herp, we hypothesized that translocation of BspL during *Brucella* infection modulates the ERAD machinery to control aBCV formation and prevent premature bacterial egress from infected cells. To test this hypothesis, we next analyzed aBCV formation in cells depleted for Herp. We took advantage of our HeLa cell model, in which aBCVs can still be monitored, although the vacuoles formed are much smaller in size (20). We first confirmed that BspL was also implicated in aBCV formation in this cell type by quantifying the number of cells containing aBCVs. We found that at 48 h postinfection, a strain lacking *bspL* formed significantly more aBCVs than the wild-type and complemented strains (Fig. 5*A*), as we observed for iBMDM.

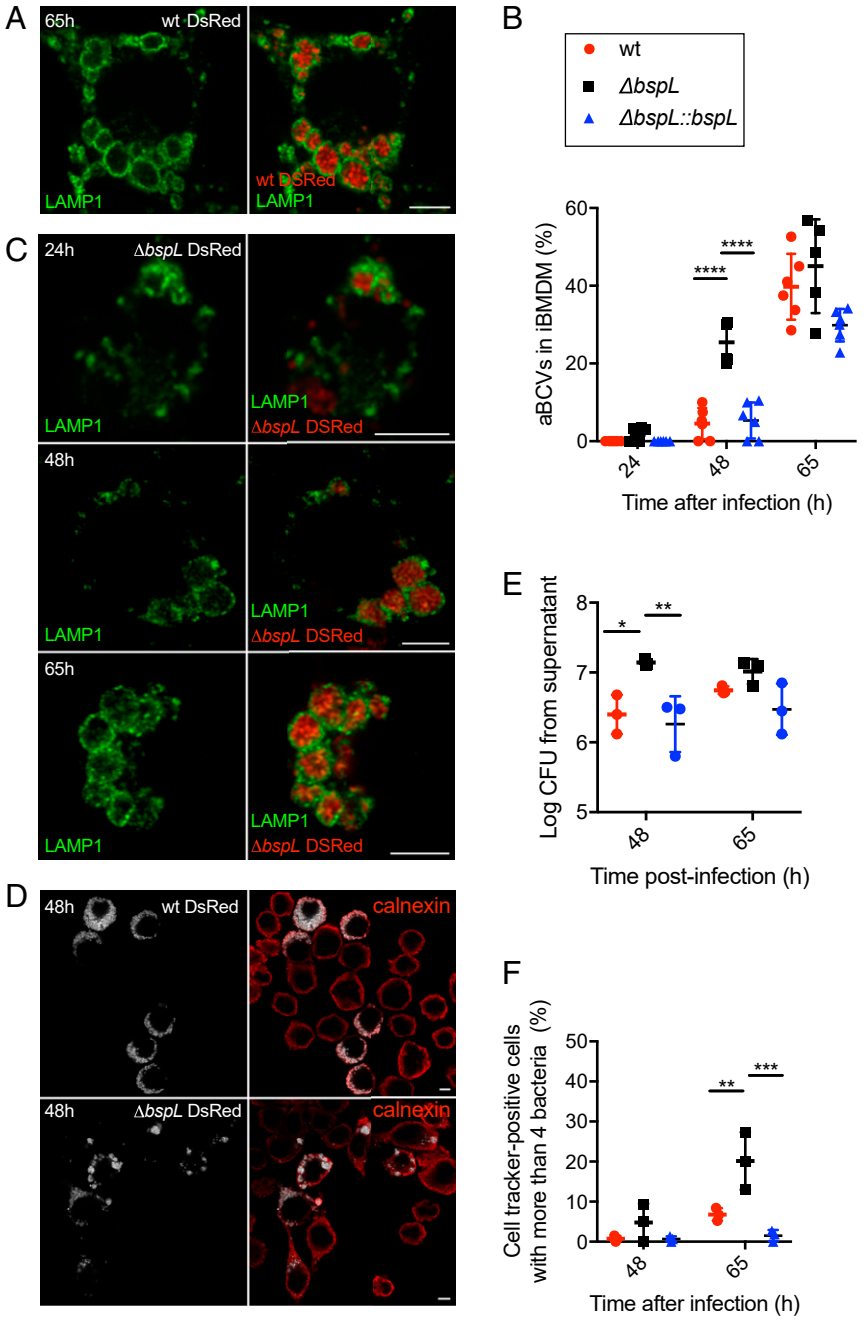

Fig. 4. BspL is implicated in a delay of aBCV formation. (*A*) Representative confocal images of iBMDM infected with wild-type DSred for 65 h labeled for LAMP1 (green). (Scale bar, 5 μm.) (*B*) Quantification of the percentage of cells with aBCVs, in iBMDMs infected with either wild-type, Δ*bspL*, or the complemented Δ*bspL::bspL* strains for 24, 48, or 65 h. Data correspond to means ± SD from five independent experiments. A two-way ANOVA was used, yielding a $P < 0.0001$ (****) between wild-type and Δ*bspL* as well as Δ*bspL* and Δ*bspL::bspL* at 48 h. Other comparisons are not indicated. (*C*) Representative confocal images of iBMDM infected with Δ*bspL* DSred for 24 h (*Top*), 48 h (*Middle*) and 65 h (*Bottom*), labeled for LAMP1 (green). (Scale bars, 5 μm.) (*D*) Representative confocal image of iBMDM infected with either wild-type DSRed or Δ*bspL* for 48 h, labeled for calnexin (red). Bacteria are shown in white. (Scale bars, 5 μm.) (*E*) Enumeration of bacterial CFU counts in the supernatants recovered at 48 or 65 h postinfection in HeLa cells infected with either wild-type, Δ*bspL,* or the complemented Δ*bspL::bspL* strains. Data correspond to means ± SD from three independent experiments. A two-way ANOVA was used yielding a $P = 0.0115$ (*) between wild-type and Δ*bspL* and 0.0036 (**) between Δ*bspL* and Δ*bspL::bspL* at 48 h. All other comparisons gave rise to $P > 0.05$. (*F*) Quantification of the percentage of infected Cell Tracker green-labeled cells at 48 or 65 h postinfection in HeLa cells infected with either wild-type, Δ*bspL,* or the complemented Δ*bspL::bspL* strains. Data correspond to means ± SD from three independent experiments. A two-way ANOVA was used yielding a $P = 0.0019$ (**) between wild-type and Δ*bspL* and 0.0001 (***) between Δ*bspL* and Δ*bspL::bspL* at 65 h. All other comparisons gave rise to $P > 0.05$.

As early blocking of ERAD could impact early trafficking events, we decided to inhibit Herp at 24 h postinfection to allow the regular establishment of rBCVs. Interestingly, we found that inhibition of Herp at 24 h postinfection resulted in a higher percentage of cells with aBCVs being formed at 48 h compared to siControl-treated cells (Fig. 5*C*), mimicking the results obtained with Δ*bspL*. Furthermore, depletion of another critical ERAD component, Hrd, also increased the number of cells with

aBCVs at 48 h postinfection, showing that blocking of ERAD impacts aBCV formation (Fig. 5*C*). Finally, to test if these results could be transposed to macrophages, we treated iBMDM between 24 and 48 h with kifunensin, a specific inhibitor of class I α-mannosidases essential for ERAD, which also resulted in enhanced aBCV formation after 48 h postinfection (Fig. 5*D*). Therefore, we propose that BspL delays aBCV appearance by directly modulating Herp functions and inducing ERAD during infection (Fig. 5*E*).

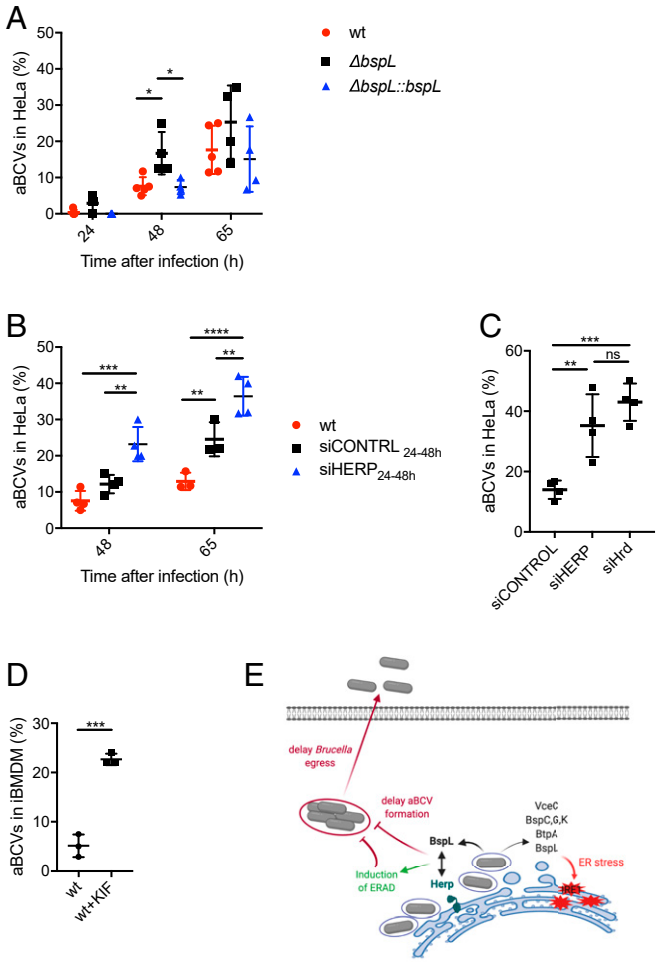

Fig. 5. Delay of aBCV formation is dependent on Herp. (*A*) Quantification of the percentage of cells with aBCVs in HeLa cells infected with either wild-type, Δ*bspL,* or the complemented Δ*bspL::bspL* strains for 24, 48, or 65 h. Data correspond to means ± SD from four independent experiments. A two-way ANOVA was used yielding a $P = 0.0422$ (*) between wild-type and Δ*bspL* and $P = 0.0445$ (*) for Δ*bspL* and Δ*bspL::bspL* at 48 h. (*B*) Quantification of the percentage of cells with aBCVs, in HeLa cells infected with wild-type *B. abortus* for 48 or 65 h with either siControl or siHerp added at 24 h postinfection. A two-way ANOVA was used yielding a $P = 0.0001$ (***) between wild-type (wt) and wt+siHerp and $P = 0.0031$ (**) for wt+siControl and wt+siHerp at 48 h. In the case of 65 h, $P < 0.0001$ (****) between wild-type (wt) and wt+siHerp and $P = 0.0032$ (**) for wt+siControl and wt+siHerp. A nonspecific effect of the siControl was observed at this time point in relation to untreated cells $P = 0.0063$. (*C*) Percentage of HeLa cells with wild-type aBCVs in siControl-, siHERP-, or siHrd-treated cells. siRNAs were added at 24 h postinfection, and cells fixed 24 h later. Data correspond to means ± SD from four independent experiments, and a one-way ANOVA was used for comparisons, with $P = 0.0048$ between siControl and siHERP (**) and 0.0009 with siHrd (***). (*D*) Percentage of iBMDM presenting aBCVs following infection with wild-type *B. abortus* with (wt+KIF) or without treatment with kifunensin (KIF) (wt) from 24 to 48 h. Data correspond to means ± SD from three independent experiments. (*E*) Model of BspL functions. Translocated BspL interacts with Herp leading to the induction of ERAD and delaying the formation of aBCVs. This results in the delay of bacterial exit from infected cells and dissemination. BspL translocation also results in enhanced ER stress along with other ER-targeting effectors.

Discussion

In this study, we characterized a previously unknown T4SS effector of *B. abortus* and its role in virulence. We found this effector hijacks Herp, a component of the ERAD machinery, to regulate the late stages of the *Brucella* intracellular cycle. Although many bacterial pathogens have been shown to control UPR, very little is known about the impact of ERAD, a downstream process, in the context of intracellular bacterial infections. To our knowledge, there are only two reports (37, 38). The obligatory intracellular pathogen *Orientia tsutsugamushi*, the cause of scrub typhus, is an auxotroph for histidine and aromatic amino acids and was shown to transiently induce UPR and block ERAD during the first 48 h of infection. This, in turn, enables the release of amino acids in the cytosol, necessary for its growth (37). The second example is *Legionella pneumophila*, which recruits the AAA ATPase Cdc48/p97 to its vacuole, which generally recognizes ubiquitinated substrates and can act as a chaperone in the context of ERAD to deliver misfolded proteins to the proteasome. Recruitment of Cdc48/p97 to the *Legionella* vacuole is necessary for intracellular replication and helps dislocate ubiquitinated proteins from the vacuolar membrane, including bacterial effectors (38).

In the case of BspL, we found it directly interacts with Herp, a component of ERAD. Our data suggest that BspL boosts ERAD, both when transiently ectopically expressed in cells and during the late stages of the infection. We could not directly show that BspL-mediated ERAD induction is dependent on Herp as its depletion would itself block ERAD (11, 39). Identification of interacting domains will help test this hypothesis by allowing the construction of mutant strains unable to interact with Herp. Nonetheless, the BspL ERAD-inducing phenotype prompted us to further investigate ERAD and Herp roles during *Brucella* infection. We found that BspL did not affect the early stages of intracellular trafficking, allowing *B. abortus* to establish its ER-derived replicative niche. However, a significant impact in the kinetics of aBCV formation was observed in the absence of BspL, depletion of Herp, or following ERAD inhibition.

These results suggest that the presence of BspL and its ability to modulate Herp functions and ERAD could provide a regulatory mechanism for the late stages of the *Brucella* life cycle. Indeed, we observed that mutants lacking BspL are released prematurely from cells, leading to earlier cell-to-cell spread. BspL action may ensure that *B. abortus* has enough time to replicate intracellularly before egressing from host cells and spreading within the tissue. It is possible that premature egress could be detrimental to host colonization. If this was the case, a mutant lacking BspL could show decreased virulence in a whole organism. We attempted to test the relevance of aBCV formation and regulation of its kinetics in vivo, using an intranasal infection model, but we could not detect any differences in lung colonization at 2 or 5 d postinfection. It is possible that the difference in kinetics observed in vitro may not translate to dissemination differences in vivo, as the wild-type strain does reach the same levels of aBCVs being formed at 65 h. It is also possible that a slower aBCV formation would benefit dissemination in other tissues or even systemically, which would require a more detailed analysis of the kinetics of infection. Finally, it is likely that other effectors may participate in this regulation and would therefore mask the *bspL* phenotype. Further work is now necessary to establish the relevance of aBCV formation in vivo and whether its tight regulation could be contributing to tissue dissemination.

It is still unclear what the precise mechanisms that enable BspL to facilitate ERAD are. It is possible that BspL interaction

with Herp stabilizes it, preventing its degradation, and would therefore help sustain ERAD. Indeed, ER stress significantly induces Herp levels, but Herp was shown to be quickly degraded, enabling efficient modulation of ERQC (40). Alternatively, BspL may favor Herp accumulation at ERQC sites that would enhance its ability to assist protein retrotranslocation and delivery to proteasomes. Herp depletion has been shown to up-regulate Beclin-1, suggesting Herp can act as an autophagy regulator (41). It is, therefore, possible that the transient presence of BspL at a particular time frame of the *Brucella* intracellular cycle could stabilize Herp and lead to down-regulation of Beclin-1 activity, which is essential for aBCV formation (20).

We found BspL itself was implicated in the induction of UPR. However, this phenotype was independent of Herp in vitro and may be an indirect effect due to the ER accumulation of BspL. Alternatively, BspL may interact with additional cellular targets. Furthermore, the increased ERAD activity upon BspL expression was not a result of high ER stress, suggesting that BspL independently controls these two pathways. There is growing evidence that the induction of IRE1-dependent UPR by multiple effectors is linked to the modulation of *Brucella* intracellular trafficking and intracellular multiplication (14, 19). Our data allow us to add another piece to this complex puzzle and place the ERAD pathway at the center of *Brucella* regulation of its intracellular trafficking. In conclusion, our results show that Herp modulation by BspL enables *Brucella* to temporarily delay the formation of aBCVs and avoid early egress from infected cells, highlighting a mechanism for fine-tuning of bacterial pathogen intracellular trafficking.

Material and Methods

Cell Culture. HeLa, RAW, and HEK293T cells obtained from ATCC were grown in DMEM supplemented with 10% of fetal calf serum. iBMDM from C57BL/6J mice were obtained from Thomas Henry, Centre International de Recherche en Infectologie, Lyon, France, and were maintained in DMEM supplemented with 10% FCS and 10% spent medium from L929 cells that supply MC-CSF.

Transfections and siRNA. All cells were transiently transfected using Torpedo (Ibidi-Invitrogen) for 24 h, according to the manufacturer's instructions. siRNA experiments were done with Lipofectamine RNAiMAX Reagent (Invitrogen) according to the protocol of the manufacturers. Importantly, siRNA depletion of Herp was done by treatment with 3 μM siRNA the day after seeding of cells and again at 24 h. Depletion was achieved after 48 h total. Depletion was confirmed by Western blotting with an antibody against Herp. ON-TARGETplus siRNA SMARTpool (L-020918) was used for Herp and, for the control, ON-TARGETplus Nontargeting pool (D-001810) both from Dharmacon. For both transfections and siRNA, cells were seeded 18 h at 2×10^4 cells per well and 1×10^5 cells per well for 24- and 6-well plates, respectively.

Bacterial Strains and Growth Conditions. *B. abortus* 2308 was used in this study. Wild-type and derived strains were routinely cultured in liquid tryptic soy broth and agar; 50 μg/mL kanamycin was added for cultures of DSRed-expressing bacteria.

Construction of BspL Eukaryotic Expression Vectors. The BspL constructs were obtained by cloning in the gateway pDONR (Life Technologies) and then cloned in the pENTRY Myc, HA or GFP vectors. Details are provided in *SI Appendix, Supplementary Materials and Methods*.

Construction of *bspL* Mutant and Complementing Strain. *B. abortus* 2308 knockout mutant Δ*bspL* was generated by allelic replacement and the complementing strain was constructed by amplifying BspL and its promoter region (500 bp upstream). Details are provided in *SI Appendix, Supplementary Materials and Methods*.

HA-TCRα. The pcDNA-TCRα was obtained from Linda Hendershot, St. Jude's Children's Research Hospital, Memphis, TN, and it corresponds to the A6-TCRα (34). The HA tag was introduced by sequence and ligation independent cloning method into pcDNA3.1 as described in *SI Appendix, Supplementary Materials and Methods*. The in vitro experiments to evaluate ERAD using HA-TCRα are described in *SI Appendix, Supplementary Materials and Methods*.

ERAD Substrate NHK–α1-Antitrypsin. cDNA encoding the NHK mutant of α1-antitrypsin (provided by Thomas Rutkwski, University of Iowa, Iowa City, IA) (42) was HA-tagged, amplified and cloned into pCMV-Myc (Clontech) as described in *SI Appendix, Supplementary Materials and Methods*. The in vitro experiments to evaluate ERAD using this vector are described in *SI Appendix, Supplementary Materials and Methods*.

Infections. Bacterial cultures were incubated for 16 h from isolated colonies in TSB shaking overnight at 37 °C. Culture optical density was controlled at 600 nm. Bacterial cultures were diluted to obtain the appropriate multiplicity of infection (MOI) for HeLa 1:500 and iBMDMs 1:50 in the appropriate medium. Infected cells were centrifuged at $400 \times g$ for 10 min to initiate bacterial–cell contact, followed by incubation for 1 h at 37 °C and 5% CO_2 for HeLa cells and 15 min for iBMDMs. After the cells were washed three times with DMEM and treated with gentamycin (50 μg/mL) to kill extracellular bacteria for 1 h. At 2 h postinfection, the medium was replaced with a weaker gentamycin concentration of 10 μg/mL. Cells were plated 18 h before infection and seeded at 2×10^4 cell per well and 1×10^5cells per well for 24- and 6-well plates, respectively. For real-time quantitative PCR experiments, 10-mm cell culture plates were used at a density of 1×10^6 cells per plate. At the different time points, cells were either harvested or coverslips fixed for immunostaining. In the case of bacterial cell counts, cells were lysed in 0.1% Triton for 5 min and a serial dilution plated for enumeration of bacterial CFU.

For enumeration of bacterial CFU counts in the supernatant, the antibiotic was removed from the media 24 h before collecting the supernatant.

Cell-to-Cell Spread Assay. HeLa cells were seeded overnight at 1.8×10^4 cells per well in 24-well plates with glass coverslips and infection carried out as described above with an MOI of 300. The next day, fresh HeLa cells were prelabeled with 2 mM Cell Tracker green CMFDA (5-chloromethylfluorescein diacetate; Life Technologies) for 30 min at 37 °C, washed three times with PBS, harvested with trypsin, and added to infected cells at the concentration of 1×10^4 green-labeled cells per well. After 4 h of adhesion, fresh media was added without antibiotics, and cells were then fixed 20 h later, corresponding to either 48 h or 65 h postinfection. The percentage of green-labeled cells infected cells was established by counting green-labeled cells with more than four bacteria when present in the vicinity of nonlabeled infected cells.

Immunofluorescence Microscopy. At the appropriate time point, coverslips were washed twice with PBS, fixed with AntigenFix (MicromMicrotech France) for 15 min, and then rewashed four times with PBS. For ER and Herp immunostaining, permeabilization was carried out with a solution of PBS containing 0.5% saponin for 30 min followed by also blocking for 30 min in a solution of PBS containing 1% bovine serum albumin (BSA), 10% horse serum, 0.5% saponin, 0.1% Tween, and 0.3 M glycine. Coverslips were then incubated for 3 h at room temperature or 4 °C overnight with primary antibody diluted in the blocking solution. Subsequently, the coverslips were washed twice in PBS containing 0.05% saponin and incubated for 2 h with secondary antibodies. Finally, coverslips were washed twice in PBS with 0.05% saponin, once in PBS and once in ultrapure water. Finally, they were mounted on a slide with ProLongGold (Life Technologies). The coverslips were visualized with a Confocal Zeiss inverted laser-scanning microscope LSM800 and analyzed using ImageJ software. For Lamp1 immunostaining, no prepermeabilization and blocking were done, and coverslips were directly incubated with antibody mixture diluted in PBS containing 10% horse serum and 0.5% saponin for 1 h at room temperature. The remaining protocol was the same as described above.

Western blotting protocol, antibodies, and drug treatments are described in *SI Appendix, Supplementary Materials and Methods*.

TEM1 Translocation Assay. RAW cells were seeded in 96-well plates at 1×10^4 cells per well overnight. Cells were then infected with an MOI of 300 by centrifugation at 4 °C, $400 \times g$ for 5 min and 1 at 37 °C 5% CO_2. Cells were washed with HBSS containing 2.5 mM probenecid. Then CCF2 mix (as described in the Life Technologies protocol) and probenecid were added to each well and incubated for 1.5 h at room temperature in the dark. Cells were finally washed with PBS, fixed using Antigenfix, and analyzed immediately by confocal microscopy (Zeiss LSM800).

RNA Isolation and Real-Time Quantitative PCR. HeLa cells were seeded in 100 mm diameter culture dishes at 1×10^6 cells per plate for each condition and were transfected with HA-tagged BspL, VceC, or BspB for 24 h or infected with wild-type, mutant, or complemented strains for 48 h. Cells were then washed 1× in PBS, scrapped in buffer RLT (Qiagen) supplemented with

β-mercaptoethanol, and transferred on a Qiashredder column (Qiagen). Several wash steps were performed and total RNAs were extracted using an RNeasy Mini Kit (Qiagen). Next, 500 ng of RNA were reverse-transcribed in a final volume of 20 μL using QuantiTect Reverse Transcription Kit (Qiagen). Real-time PCR was performed using SYBR Green PowerUp (ThermoScientific) with a QuantiTect Studio 3 (ThermoScientific). The *HPRT* and *GAPDH* expressions were used as internal controls for normalization and fold-change calculated in relation to the negative control. Specific primers are indicated in *SI Appendix, Supplementary Materials and Methods*.

Secretion Assay. HEK293T cells were harvested and seeded in six-well plates at 1×10^5 cells per well and cotransfected with plasmids encoding *Brucella* secreted proteins (300 ng DNA) and the SEAP (300 ng DNA). The total amount of transfected DNA was maintained constant using an empty vector pcDNA 3.1 for the positive control. At 18 h posttransfection, the transfection media was removed and then cells were still incubated at 37 °C 5% CO_2. Forty-eight hours later, media containing culture supernatant (extracellular SEAP) was removed and collected. To obtain intracellular SEAP, each well was washed with PBS and then incubated with a solution of PBS-Triton X-100 0.5% for 10 min. Incubation of each fraction was performed at 65 °C following centrifugation at maximum speed for 30 s. Then, cells were incubated with a provided substrate 3-(4-methoxyspiro [1,2-dioxetane-3,2′(5′-chloro)-tricyclo(3.3.1.13,7) decane]-4-yl)phenyl phosphate (CSPD) by SEAP reporter gene assay, chemiluminescent kit (Roche Applied Science). Chemiluminescence values were obtained with the use of a TECAN at 492 nm. Data are presented as the SEAP secretion index, a ratio of extracellular SEAP activity to intracellular SEAP activity.

Yeast Two-Hybrid. BspL was cloned into pDBa vector, using the Gateway technology, transformed into MaV203 and used as a bait to screen a human embryonic brain cDNA library (Invitrogen). Media, transactivation test, screening assay, and gap repair test were performed as described previously (43–45).

Co-IP. HeLa cells were cultured in 100 mm diameter cell culture dishes at 1×10^6 cells per dish overnight. Cells were transiently transfected with 30 μL of Torpedo^{DNA} (Ibidi) for 24 h for a total of 10 μg of DNA per plate. On ice, after two washes with cold PBS, cells were collected with a cell scraper and centrifuged at $80 \times g$ at 4 °C for 10 min. Cell lysis and processing for co-IP were done as described with the PierceTM HA Epitope Antibody Agarose conjugate (Thermo scientific) or GFP-Trap (Chromotek).

Murine Infection Model. Wild-type C57BL/6 mice were acquired from Harlan (Bicester) and were bred in the animal facility of the Gosselies campus of the Université Libre de Bruxelles (Belgium). Mice were infected intranasally by wild-type or BspL *B. abortus* 2308 in PBS. The infectious doses were validated by plating serial dilutions of the inoculums. Mice were anesthetized with a mixture of Xylasine (9 mg/kg) and Ketamine (36 mg/kg) in PBS before being inoculated intranasally with 30 μL of the indicated dose of *B. abortus*.

The procedures used in this study and the handling of the mice complied with current European legislation (Directive 86/609/EEC) and the corresponding Belgian law "Arrêté royal relatif à la protection des animaux d'expérience" of 6 April 2010 and published on 14 May 2010. The Animal Welfare Committee of the Université de Namur (Belgium) reviewed and approved the complete protocol for *Brucella melitensis* infection (Permit no. UN-LE-13/195).

Statistical Analysis. All datasets were tested for normality using the Shapiro–Wilkinson test. When a normal distribution was confirmed, we used a one-way ANOVA test with a Dunnett correction for statistical comparison of multiple datasets with the negative control or Tukey's correction for multiple comparisons. For two independent variables, a two-way ANOVA test was used. For datasets that did not show normality, a Kruskal–Wallis test was applied, with Dunn's correction, or Mann–Whitney *U* test for two-sample comparison. All analyses were done using Prism Graph Pad 7.

Data Availability. All study data are included in the article and *SI Appendix*.

ACKNOWLEDGMENTS. We thank Linda Hendershot (St. Jude's Children's Research Hospital) for sending us the pcDNA-TCRα and for all the help with setting up the endoplasmic reticulum-associated degradation assay and discussion of the results; Thomas Rutkowski (University of Iowa) for the cDNA encoding the Null Hong Kong mutant of α1-antitrypsin; Renée Tsolis (University of California, Davis) for help constructing TEM1-VceC and HA-VceC; Thomas Henry (Centre International de Recherche en Infectologie, Lyon, France) for the immortalized cell line of bone marrow-derived macrophages; Steve Garvis, Amandine Blanco, and Arthur Louche for the critical reading of the manuscript; and Peter Cresswell and Susan Mitchell (Yale University School of Medicine) for sending us the endoplasmic reticulum-associated degradation reporter cell line and all the advice despite all the challenges imposed by the pandemic. All microscopy imaging was carried out at the PLATIM microscopy facility. The two-hybrid screening was hosted by the Marseille Proteomics platform (J.-P.B. and F.L.) supported by Institut Paoli-Calmettes, Infrastructures Biologie Santé et Agronomie, Aix-Marseille University, Canceropôle PACA, and the Région Sud Provence-Alpes-Côte d'Azur. J.-P.B. is a scholar of Institut Universitaire de France. This work was funded by the ERA-Net Pathogenomics CELLPATH Grant Agriculture and Natural Resources (ANR) 2010-PATH-006, the FINOVI foundation under a Young Researcher Starting grant, ANR NUCPATH Grant ANR-15-CE15-0011, and the ANR charm-Ed Grant ANR-18-CE15-0003 (all obtained by S.P.S.). J.-B.L. was supported by a doctoral contract from the Région Rhônes-Alpes ARC1 Santé. An INSERM staff scientist contract supports S.P.S. The original submission of this manuscript was published on BiorXiv and is part of the PhD thesis manuscript of J.-B.L., "Host Cell modulation by *Brucella* effectors," Université de Lyon, France, 2019.

1. I. Braakman, N. J. Bulleid, Protein folding and modification in the mammalian endoplasmic reticulum. *Annu. Rev. Biochem.* **80**, 71–99 (2011).
2. X. Wu, T. A. Rapoport, Mechanistic insights into ER-associated protein degradation. *Curr. Opin. Cell Biol.* **53**, 22–28 (2018).
3. P. Walter, D. Ron, The unfolded protein response: From stress pathway to homeostatic regulation. *Science* **334**, 1081–1086 (2011).
4. K. Kokame, K. L. Agarwala, H. Kato, T. Miyata, Herp, a new ubiquitin-like membrane protein induced by endoplasmic reticulum stress. *J. Biol. Chem.* **275**, 32846–32853 (2000).
5. Y. Ma, L. M. Hendershot, Herp is dually regulated by both the endoplasmic reticulum stress-specific branch of the unfolded protein response and a branch that is shared with other cellular stress pathways. *J. Biol. Chem.* **279**, 13792–13799 (2004).
6. S. L. Chan *et al*., Herp stabilizes neuronal Ca2+ homeostasis and mitochondrial function during endoplasmic reticulum stress. *J. Biol. Chem.* **279**, 28733–28743 (2004).
7. S. Tuvia *et al*., The ubiquitin E3 ligase POSH regulates calcium homeostasis through spatial control of Herp. *J. Cell Biol.* **177**, 51–61 (2007).
8. J. Leitman *et al*., Herp coordinates compartmentalization and recruitment of HRD1 and misfolded proteins for ERAD. *Mol. Biol. Cell* **25**, 1050–1060 (2014).
9. C.-H. Huang, Y.-R. Chu, Y. Ye, X. Chen, Role of HERP and a HERP-related protein in HRD1-dependent protein degradation at the endoplasmic reticulum. *J. Biol. Chem.* **289**, 4444–4454 (2014).
10. M. Kny, S. Standera, R. Hartmann-Petersen, P.-M. Kloetzel, M. Seeger, Herp regulates Hrd1-mediated ubiquitylation in a ubiquitin-like domain-dependent manner. *J. Biol. Chem.* **286**, 5151–5156 (2011).
11. Y. Okuda-Shimizu, L. M. Hendershot, Characterization of an ERAD pathway for nonglycosylated BiP substrates, which require Herp. *Mol. Cell* **28**, 544–554 (2007).
12. J. Celli, R. M. Tsolis, Bacteria, the endoplasmic reticulum and the unfolded protein response: Friends or foes? *Nat. Rev. Microbiol.* **13**, 71–82 (2015).
13. M. F. de Jong *et al*., Sensing of bacterial type IV secretion via the unfolded protein response. *mBio* **4**, e00418-12 (2012).
14. J. A. Smith *et al*., Brucella induces an unfolded protein response via TcpB that supports intracellular replication in macrophages. *PLoS Pathog.* **9**, e1003785 (2013).
15. A. M. Keestra-Gounder *et al*., NOD1 and NOD2 signalling links ER stress with inflammation. *Nature* **532**, 394–397 (2016).
16. Q.-M. Qin *et al*., RNAi screen of endoplasmic reticulum-associated host factors reveals a role for IRE1alpha in supporting *Brucella* replication. *PLoS Pathog.* **4**, e1000110 (2008).
17. T. Starr, T. W. Ng, T. D. Wehrly, L. A. Knodler, J. Celli, Brucella intracellular replication requires trafficking through the late endosomal/lysosomal compartment. *Traffic* **9**, 678–694 (2008).
18. J. Sedzicki *et al*., 3D correlative electron microscopy reveals continuity of *Brucella*-containing vacuoles with the endoplasmic reticulum. *J. Cell Sci.* **131**, jcs210799 (2018).
19. Y. Taguchi *et al*., Yip1A, a novel host factor for the activation of the IRE1 pathway of the unfolded protein response during *Brucella* infection. *PLoS Pathog.* **11**, e1004747 (2015).
20. T. Starr *et al*., Selective subversion of autophagy complexes facilitates completion of the *Brucella* intracellular cycle. *Cell Host Microbe* **11**, 33–45 (2011).
21. R. M. Delrue *et al*., Identification of *Brucella* spp. genes involved in intracellular trafficking. *Cell Microbiol.* **3**, 487–497 (2001).
22. D. J. Comerci, M. J. Martínez-Lorenzo, R. Sieira, J. P. Gorvel, R. A. Ugalde, Essential role of the VirB machinery in the maturation of the Brucella abortus-containing vacuole. *Cell Microbiol.* **3**, 159–168 (2001).
23. J. Celli *et al*., *Brucella* evades macrophage killing via VirB-dependent sustained interactions with the endoplasmic reticulum. *J. Exp. Med.* **198**, 545–556 (2003).
24. E. P. Smith, C. N. Miller, R. Child, J. A. Cundiff, J. Celli, Postreplication roles of the *Brucella* VirB type IV secretion system uncovered via conditional expression of the VirB11 ATPase. *MBio* **7**, 215 (2016).

25. S. Myeni *et al*., *Brucella* modulates secretory trafficking via multiple type IV secretion effector proteins. *PLoS Pathog.* **9**, e1003556 (2013).
26. C. N. Miller *et al*., A Brucella type IV effector targets the COG tethering complex to remodel host secretory traffic and promote intracellular replication. *Cell Host Microbe* **22**, 317–329.e7 (2017).
27. E. Boucrot, C. R. Beuzón, D. W. Holden, J.-P. Gorvel, S. Méresse, *Salmonella typhimurium* SifA effector protein requires its membrane-anchoring C-terminal hexapeptide for its biological function. *J. Biol. Chem.* **278**, 14196–14202 (2003).
28. A. T. Reinicke *et al*., A Salmonella typhimurium effector protein SifA is modified by host cell prenylation and S-acylation machinery. *J. Biol. Chem.* **280**, 14620–14627 (2005).
29. C. T. D. Price, T. Al-Quadan, M. Santic, S. C. Jones, Y. Abu Kwaik, Exploitation of conserved eukaryotic host cell farnesylation machinery by an F-box effector of *Legionella pneumophila*. *J. Exp. Med.* **207**, 1713–1726 (2010).
30. M. F. de Jong, Y.-H. Sun, A. B. den Hartigh, J. M. van Dijl, R. M. Tsolis, Identification of VceA and VceC, two members of the VjbR regulon that are translocated into macrophages by the *Brucella* type IV secretion system. *Mol. Microbiol.* **70**, 1378–1396 (2008).
31. M. I. Marchesini, C. K. Herrmann, S. P. Salcedo, J.-P. Gorvel, D. J. Comerci, In search of *Brucella abortus* type IV secretion substrates: Screening and identification of four proteins translocated into host cells through VirB system. *Cell Microbiol.* **13**, 1261–1274 (2011).
32. R. Serrat *et al*., The non-canonical Wnt/PKC pathway regulates mitochondrial dynamics through degradation of the arm-like domain-containing protein Alex3. *PLoS One* **8**, e67773 (2013).
33. T.-Y. Kim, E. Kim, S. K. Yoon, J.-B. Yoon, Herp enhances ER-associated protein degradation by recruiting ubiquilins. *Biochem. Biophys. Res. Commun.* **369**, 741–746 (2008).
34. M. J. Feige, L. M. Hendershot, Quality control of integral membrane proteins by assembly-dependent membrane integration. *Mol. Cell* **51**, 297–309 (2013).
35. J. Lippincott-Schwartz, J. S. Bonifacino, L. C. Yuan, R. D. Klausner, Degradation from the endoplasmic reticulum: Disposing of newly synthesized proteins. *Cell* **54**, 209–220 (1988).
36. J. E. Grotzke, Q. Lu, P. Cresswell, Deglycosylation-dependent fluorescent proteins provide unique tools for the study of ER-associated degradation. *Proc. Natl. Acad. Sci. U.S.A.* **110**, 3393–3398 (2013).
37. K. G. Rodino *et al*., Orientia tsutsugamushi modulates endoplasmic reticulum-associated degradation to benefit its growth. *Infect. Immun.* **86** , e00596-17 (2017).
38. M. S. Dorer, D. Kirton, J. S. Bader, R. R. Isberg, RNA interference analysis of *Legionella* in *Drosophila* cells: Exploitation of early secretory apparatus dynamics. *PLoS Pathog.* **2**, e34 (2006).
39. O. Hori *et al*., Role of Herp in the endoplasmic reticulum stress response. *Genes Cells* **9**, 457–469 (2004).
40. L. Yan *et al*., Ube2g2-gp78-mediated HERP polyubiquitylation is involved in ER stress recovery. *J. Cell Sci.* **127**, 1417–1427 (2014).
41. C. Quiroga *et al*., Herp depletion protects from protein aggregation by up-regulating autophagy. *Biochim. Biophys. Acta* **1833**, 3295–3305 (2013).
42. J. C. Christianson, T. A. Shaler, R. E. Tyler, R. R. Kopito, OS-9 and GRP94 deliver mutant alpha1-antitrypsin to the Hrd1-SEL1L ubiquitin ligase complex for ERAD. *Nat. Cell Biol.* **10**, 272–282 (2008).
43. T. L. Orr-Weaver, J. W. Szostak, Yeast recombination: The association between double-strand gap repair and crossing-over. *Proc. Natl. Acad. Sci. U.S.A.* **80**, 4417–4421 (1983).
44. S. Thalappilly *et al*., Identification of multi-SH3 domain-containing protein interactome in pancreatic cancer: A yeast two-hybrid approach. *Proteomics* **8**, 3071–3081 (2008).
45. A. J. Walhout, M. Vidal, High-throughput yeast two-hybrid assays for large-scale protein interaction mapping. *Methods* **24**, 297–306 (2001).